Structural analysis of human alpha-class glutathione transferase A1-1 in the apo-form and in complexes with ethacrynic acid and its glutathione conjugate

Alexander D Cameron[1], Irmgard Sinning[1], Guillaume L'Hermite[1], Birgit Olin[2], Philip G Board[3], Bengt Mannervik[2] and T Alwyn Jones[1]*

[1]Department of Molecular Biology, Uppsala University, Biomedical Center, Box 590, S-751 24 Uppsala, Sweden, [2]Department of Biochemistry, Uppsala University, Biomedical Center, Box 576, Uppsala, Sweden and [3]Molecular Genetics Group, John Curtin School of Medical Research, Australian National University, GPO Box 334, Canberra 2601, Australia

Background: Glutathione transferases (GSTs) constitute a family of isoenzymes that catalyze the conjugation of the tripeptide glutathione with a wide variety of hydrophobic compounds bearing an electrophilic functional group. Recently, a number of X-ray structures have been reported which have defined both the glutathione- and the substrate-binding sites in these enzymes. The structure of the glutathione-free enzyme from a mammalian source has not, however, been reported previously.

Results: We have solved structures of a human alpha-class GST, isoenzyme A1-1, both in the unliganded form and in complexes with the inhibitor ethacrynic acid and its glutathione conjugate. These structures have been refined to resolutions of 2.5 Å, 2.7 Å and 2.0 Å respectively. Both forms of the inhibitor are clearly present in the associated electron density.

Conclusions: The major differences among the three structures reported here involve the C-terminal α-helix, which is a characteristic of the alpha-class enzyme. This helix forms a lid over the active site when the hydrophobic substrate binding site (H-site) is occupied but it is otherwise disordered. Ethacrynic acid appears to bind in a non-productive mode in the absence of the coenzyme glutathione.

Structure 15 July 1995, **3**:717–727

Key words: apo-enzyme, crystallography, ethacrynic acid, glutathione

Introduction

Glutathione transferases (GSTs; EC 2.5.1.18) catalyze the nucleophilic attack of the sulphur atom of glutathione on the electrophilic groups of a wide range of hydrophobic compounds of both endobiotic and xenobiotic origins. Through this reaction they play an important role in cellular detoxification and have been described as the most important group of enzymes involved in the metabolism of electrophilic compounds [1]. The glutathione adducts produced by the reaction generally have greater water solubility than the free compounds, facilitating their removal from the cell to be degraded to mercapturates before being excreted. Additionally, the electrophilic compounds are often, though not in all cases, rendered less toxic by the conjugation reaction. GSTs have been the subject of many reviews (e.g. [1–5]). In addition to their role in detoxification, GSTs may be involved in the intracellular storage and transport of a variety of other hydrophobic, non-substrate compounds including hormones, metabolites and drugs. They have also been the focus of considerable interest with regard to drug resistance as certain drug-resistant tumour cells have elevated levels of GSTs (see [6] for a review).

That there is such a diversity of substrates for GST is a consequence not only of the fact that individual enzymes can accommodate a wide variety of substrate molecules [2] but also of the existence of many isoenzymes [7]. The isoenzymes found in the mammalian cytosol have been grouped into four species-independent classes (alpha, pi, mu and theta) based on their substrate and inhibitor specificities, antibody cross-reactivity and primary structures [8,9]. Many substrates, however, show activity with GSTs of more than one class. The intracellular level of each isoenzyme is markedly tissue-dependent [2]; the sequence homology within a class is ~75%, whereas between classes it is in the order of 20–30%.

The fully functional enzymes are dimers of molecular weight ~50000 Da. The dimers can be formed either from identical monomers or from different monomers within the same class of isoenzyme [10]. No cross-class heterodimers, however, have been discovered. Over the past few years, structures have been reported of the enzymes from the pi [11–13], mu [14–17] and alpha [18] classes (see [4,5,18] for reviews and structural comparisons). Recently, two structures of GSTs from non-mammalian sources have also been elucidated: a GST from the Australian sheep blowfly, *Lucilia cuprina* [19], and one from the parasitic worm, *Schistosoma japonica* [20]. The overall structures of all these GST proteins are similar [18]. Each subunit contains two domains: an

*Corresponding author.

 ISSN 0969-2126

N-terminal α/β–domain, with βαβαββα topology, and a C-terminal α-helical domain. Within the active site, which is situated in spatially equivalent positions in all three classes (pi, mu and alpha), there are two distinct subsites: a glutathione-binding site (G-site) and a pocket in which the hydrophobic substrates bind (H-site).

In each of the structures reported, glutathione makes a network of specific interactions with polar groups from both subunits of the GST dimer. Despite the fact that the glutathione-binding pocket is only completed on dimerization, there is no evidence of cooperativity between the subunits [2,7]. Also, whereas the G-site is similar in all structures [18], the H-site shows more variation. Both the extension of a loop in domain 1 of the mu class enzymes [14] and differences among the C termini of the respective enzymes contribute to this diversity. The polypeptide chains of the enzymes from the mu and pi classes are some four to eight residues shorter than those from the alpha class, which contain an additional C-terminal α-helix. This helix packs onto the hydrophobic substrate, partially sealing it from the surrounding solvent [18].

Recently, Ji *et al.* [16] have examined the structures of a mu-class GST bound to the diastereoisomers of 9-(*S*-glutathionyl)-10-hydroxy-9,10-dihydrophenanthrene and García-Sáez *et al.* [13] have determined the structures of *S*-(*p*-nitrobenzyl) glutathione and other inhibitors bound to a GST from the pi class. These studies have contributed to defining the H-site in these two classes. To the same end, we have solved the structures of a human alpha-class GST, A1-1, complexed with the inhibitor ethacrynic acid (EA) ([2,3-dichloro-4-{2-methylene-1-oxobutyl}phenoxy]acetic acid) and its glutathione conjugate (EA–GSH). GST A1-1 is the major isoenzyme found in human liver, where it represents ~2% of the total cytosolic protein [7,21].

EA (Fig. 1a) is a potent diuretic drug which has been shown to inhibit the alpha, pi and mu classes of GST [22–24]. It is a phenoxyacetic acid compound with an α,β-unsaturated ketone moiety in the side chain. GSTs catalyze the reaction of this unsaturated bond with glutathione to form the glutathione conjugate. The reaction is particularly efficient in the pi-class enzymes [2]. Although the catalytic efficiency is somewhat poor in the alpha class, EA still acts as a good inhibitor, with I_{50} values of approximately 10 μM. These values are even lower for EA–GSH (0.8-2.8 μM) [24].

The inhibition of GST by EA has attracted particular interest with regard to drug resistance in tumour cells. It has been used to examine the role of GSTs in drug resistance *in vitro*, using cell lines [22,23,25], and colon tumour xenografts [26]. It has also been used with moderate success in Phase I clinical trials, in which the effects of administering EA to cancer patients along with the alkylating agents thiotepa or melphalan were monitored [27,28]. It is assumed that GSTs catalyze the conjugation of such alkylating agents with glutathione, rendering them ineffective as anti-cancer drugs. By administering EA along with these drugs, their rate of clearance from the body is reduced.

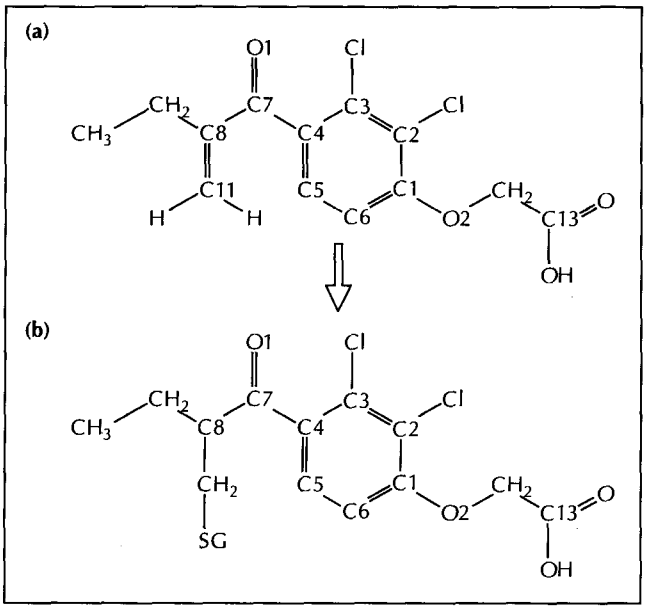

Fig. 1. Schematic representation of **(a)** EA and **(b)** EA–GSH. The glutathione moiety is represented by SG.

We report here the structures of alpha-class GST A1-1 both in the apo-form and in complexes with EA and EA–GSH. The apo-form is the first structure reported of any mammalian GST with an unoccupied G-site, though the structure of a glutathione-free GST from a parasitic worm has recently been solved [20]. In the structure of the complex with the conjugated form of glutathione, Arg15 is replaced by a lysine residue. This mutation of a residue in the active site has only a moderate effect on the catalytic properties of the enzyme and produces better-diffracting crystals [29]. Residues are numbered according to Sinning *et al.* [18] with the N-terminal alanine residue labelled Ala2.

Results and discussion

Human alpha-class glutathione A1-1 has now been crystallized both in the apo-form and in the presence of three rather different inhibitors; EA, EA–GSH and *S*-benzyl–GSH [18]. Thus we have structures of the enzyme with neither glutathione nor substrate bound, with only substrate bound (EA, in this case), and with two different glutathione conjugates, (*S*-benzyl–GSH, a relatively small inhibitor, and EA–GSH, which is bulkier and charged). This latter complex has been refined against data extending to a d_{min} of 2 Å, significantly higher than the resolution limit of the data that we have obtained for the other crystals (see the Materials and methods section and [18]). Interestingly, the crystallographic association of the dimers within this crystal is slightly altered with respect to the other structures, producing a new, but closely related, crystal form.

Crystal packing arrangement

Under the conditions used for crystallization, crystals usually grow with two dimers in the asymmetric unit that are related by an operator involving a translation of 0.5 of the unit cell along the *c* axis and a rotation of ~3°. Only small adjustments are needed, therefore, for the non-crystallographic symmetry operator to be converted into an exact crystallographic relationship, resulting in a halving of the *c* cell dimension. In the crystal of the complex with EA–GSH this is indeed what happens. Presumably, it is this optimal packing arrangement which is responsible for the better diffraction properties of the crystal.

It is unclear, however, what is responsible for the variation in crystal packing. It does not appear to be caused either by the mutation of residue 15 from arginine to lysine (Arg15→Lys) or by the presence of the EA–GSH conjugate, as we have obtained crystals of both the Arg15→Lys mutant in complex with benzyl–GSH and the wild-type enzyme in complex with EA–GSH, and these both contain two dimers in the unit cell. Furthermore, crystals of the enzyme complexed with other compounds have been seen to change from the small to the large unit cell as data collection progressed. These results suggest that the differences are caused by subtle changes in, for example, temperature or pH, however, the proximity of the H-site to crystallographically related molecules means that the ligand may also influence the crystal form. None of the residues affected by ligand binding are involved in any well defined crystal contacts. An overlay of the crystal packing arrangement in the benzyl–GSH complex onto that of the EA–GSH complex can be seen in Figure 2. One dimer of the former structure was superimposed onto the respective dimer in the latter structure by least-squares minimization of the positions of the corresponding Cα atoms. There are two main regions where relatively well defined, polar residues are involved in crystallographic interactions: residues on the loop between helices α5″ and α6 of the A molecule (helices named according to [18] and molecules of the dimer according to the EA–GSH complex, where one is labelled A and the other B) interact with residues from helices α2 and α5″ of symmetry-related A and B molecules respectively; and residues on the loop between helices α4 and α5′ of the B molecule interact with residues on helix α3 of a symmetry-related A molecule. In both of these regions the contacts are slightly different between the two crystal forms but whether the variations cause, or are a result of, the different packing is unclear. A detailed comparison of the crystal contacts is complicated by the fact that the benzyl–GSH complex was refined with strict non-crystallographic symmetry constraints.

When compared with the previously reported structure of the enzyme complexed with benzyl–GSH [18], the higher resolution of the EA–GSH complex structure contains few significant differences other than in a number of side-chain conformations and peptide orientations. The water structure is much better defined in the higher resolution complex. The overall root mean square (rms) deviations among the structures are given in Tables 1 and 2. It is evident from Table 1 that the dimer interface is not affected either by the type of inhibitor bound or by the change in crystal packing. The major variations among the molecules are localized to the C terminus. This constitutes part of the hydrophobic binding pocket (H-site) and will be dealt with below.

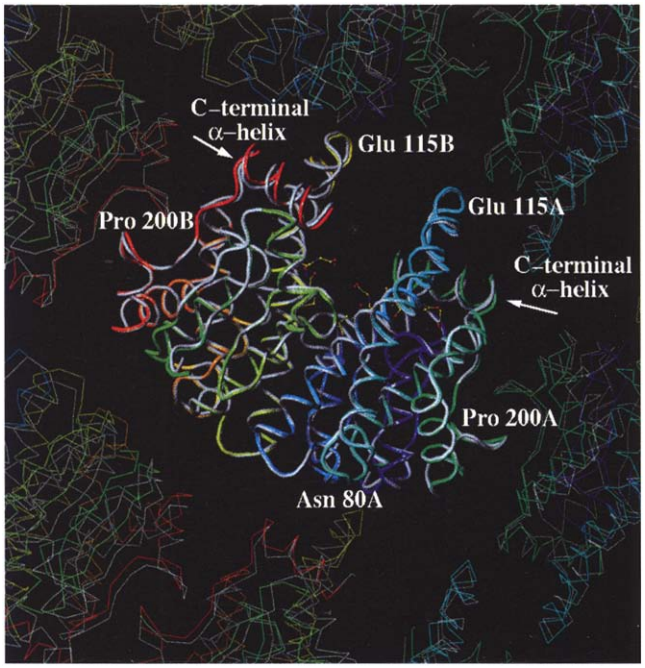

Fig. 2. Superposition of the benzyl–GSH structure and its symmetry-related molecules (grey) on the EA–GSH structure and its symmetry-related molecules (colour ramped along the dimer according to residue number, starting with blue at the N terminus and finishing with red at the C terminus). The orientation matrix was determined by least-squares superposition of the corresponding Cα atoms of one dimer, shown in thick lines in the diagram, and this was then applied to each of the tetramers in the benzyl–GSH structure. The ligand is shown in ball-and-stick representation. The view is along *b* with *c* vertical and *a* horizontal. Glu115 resides on the loop between helices α4 and α5′ and Asn80 is found just after helix α3. These regions are involved in crystallographic interactions that may affect into which cell the protein crystallizes.

Ethacrynic acid binding

In the two structures with EA (free and conjugated) bound in the H-site, the respective inhibitors can be easily located in the electron density. The protein–ligand interactions occurring in each complex will be described in turn.

EA–GSH complex

In the EA–GSH complex the glutathione moiety is well ordered and the hydrogen-bonding interactions described for the benzyl–GSH structure [18] are preserved. On the other hand, there are two conformations of the EA moiety, clearly shown (Fig. 3) by the density associated with the higher scattering chlorine atoms. The conjugation of glutathione with EA results in two possible diastereoisomers, neither of which, at least in the rat enzyme

Table 1. Rms differences (in Å) between selected atoms of the high-resolution structure of the EA–GSH complex and the other three structures.

Molecule A of EA–GSH complex	Molecule B of EA–GSH complex	Benzyl–GSH complex	EA complex	Apo-enzyme
Monomer				
All Cα atoms	0.13	0.61	0.52	0.35
Cα atoms (residues 5–207*)	0.12	0.26	0.23	0.30
All atoms	0.62	0.97	0.95	0.79
All atoms (residues 5–207)	0.47	0.69	0.68	0.75
Dimer				
Cα atoms		0.55	0.47	0.36
Cα atoms (residues 5–207)		0.28	0.21	0.32

*This excludes the three N-terminal residues, which are not well defined, and the C-terminal helix.

Table 2. Rms differences (in Å) among the respective monomers of the four structures.

Structure (residues 5–207 of the A molecule)		Benzyl–GSH complex	EA complex	Apo-enzyme
EA–GSH	main chain	0.38	0.24	0.31
	all atoms	0.69	0.68	0.75
Benzyl–GSH	main chain	–	0.36	0.34
	all atoms	–	0.69	0.72
EA	main chain	–	–	0.23
	all atoms	–	–	0.68

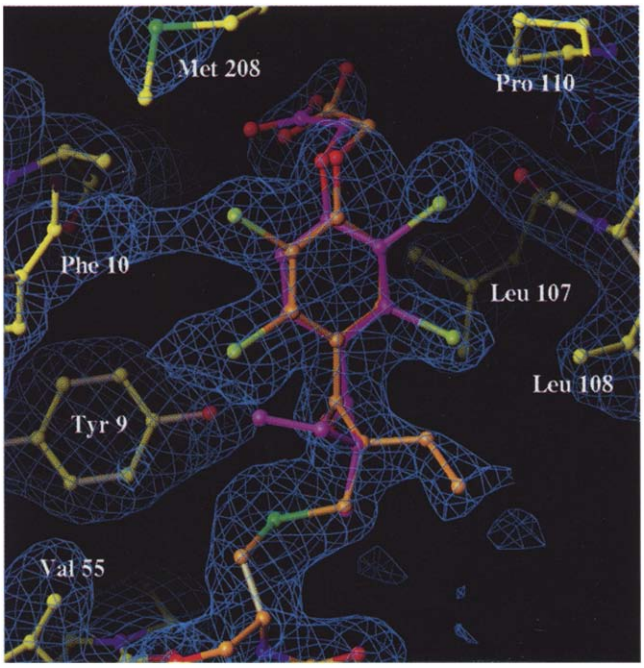

Fig. 3. $2F_o–F_c$ density associated with the ligand in the EA–GSH complex. The map was calculated using phases derived from a model in the early stages of refinement, before the inclusion of the ligand, and subjected to 10 cycles of averaging (contoured at 1σ). The two conformations of the inhibitor's EA moiety can be distinguished by the colour of their carbon atoms (magenta for one and brown for the other). The two conformations are shown modelled as different enantiomeric forms of the inhibitor. In the final structure, however, both conformations are modelled in the same enantiomeric form as the density at the site of the conjugation cannot be unambiguously interpreted (see text).

GST 33, is preferentially selected [24]. As both of th diastereoisomers should be present in the crystallization mixture, it is possible that the two conformations of the EA moiety represent different enantiomeric forms of the conjugate. As the quality of the electron density at the site of the conjugation is ambiguous, however, the two conformations of the EA moiety have been modelled such that only one enantiomer is represented in the final structure. The major difference between the two conformations is a rotation of the dichlorophenoxy group by approximately 140° around an axis which passes through both O2 and C7 (see Fig. 1 for atomic naming convention) as well as through the centre of the ring. The acidic side chains and carbonyl groups of each molecule are almost superimposed (see Fig. 4).

The interactions with GST made by the EA moiety are mainly hydrophobic in nature, with the dichlorophenoxy group in van der Waals contact with the Cα of Gly14 and the side chains of residues Phe10, Leu107, Leu108, Val111, Met208 and Phe222. Despite the hydrophobic nature of the H-site, both the carbonyl oxygen O1 (Fig. 1) and the carboxylate oxygens are involved in hydrogen-bonding interactions (Fig. 4). The carbonyl oxygen acts as a hydrogen-bond acceptor from the hydroxyl group of Tyr9 (O to OH distances range from 2.8 Å–3.3 Å among the two conformations of the EA moiety and the two molecules of the asymmetric unit). In the wild-type enzyme it would also be within potential hydrogen-bonding distance of Arg15 (Nε ~3.3 Å) assuming that the arginine residue retains the same conformation as in the benzyl–GSH complex. The carboxylate oxygens are involved in three potential hydrogen-bonding interactions, one with the amino nitrogen of Gly14 (3.0–3.2 Å) and two with water molecules (Fig. 4). One of these water molecules is conserved among all the solved GST A1-1 structures. It lies 2.8–3.4 Å from the carboxylate, has a relatively low B-value (21 $Å^2$ and 36 $Å^2$ in the A and B molecules, respectively) and makes hydrogen bonds to both the carbonyl oxygen of Pro207 (~2.9 Å) and the amino nitrogen of Arg13 (~2.7 Å). The other is less well defined (B-values of 45 $Å^2$ and 46 $Å^2$ in the A and B molecules, respectively) and on average lies further from the inhibitor (3.0–3.5 Å). These interactions show that the enzyme is able to interact with the polar atoms of the substrate, despite the hydrophobic nature of the binding site, by direct protein hydrogen bonds and hydration effects.

Ethacrynic acid complex

The electron density for EA in the substrate–enzyme complex is shown in Figure 5. In this structure, the dichlorophenoxy ring appears to adopt only one

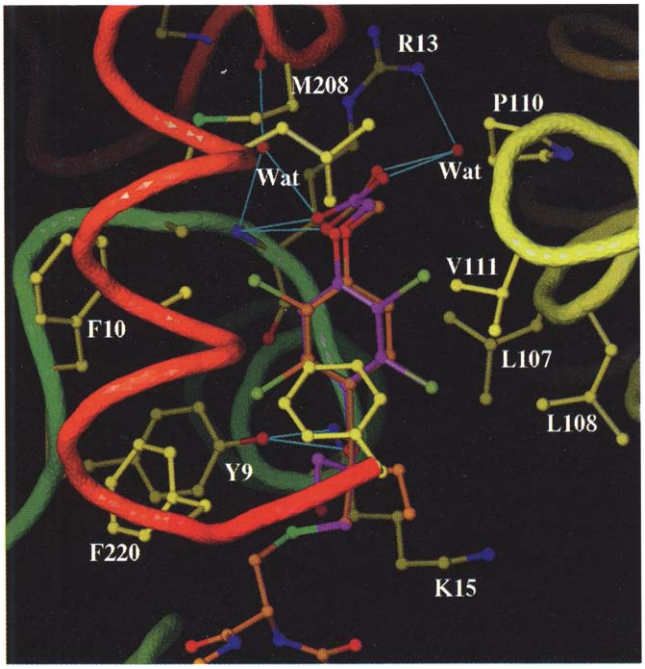

Fig. 4. View of the H-site in the EA–GSH complex. The ribbon representation of the molecule has been colour ramped according to residue number as in Figure 2. The inhibitor's EA moiety is shown in two conformations which can be differentiated by the colour of their respective carbon atoms. In one conformation the carbon atoms have been coloured brown and in the other magenta. The carbon atoms of the protein are coloured yellow. Possible hydrogen bonds are represented by cyan lines.

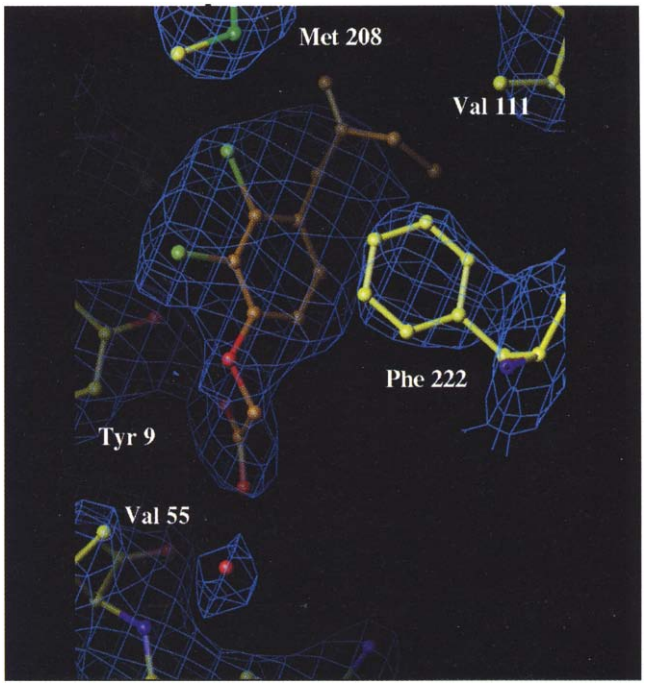

Fig. 5. $2F_o–F_c$ electron density associated with the ligand in the EA complex. The map was calculated using phases derived from a model in the early stages of refinement, before the inclusion of the ligand, and subjected to 10 cycles of averaging (contoured at 1σ). The coordinates of the final structure have been superimposed. The carbon atoms of the inhibitor are coloured brown to differentiate them from those of the protein, which are coloured yellow.

conformation. Both the shape of the density and the size similarity of the substitutions to the phenol ring make the assignment of the orientation ambiguous (see the Materials and methods section). In our preferred model, the carboxylate group is oriented towards, and partly occupies, the G-site. Indeed, one of the carboxylate oxygens lies 0.8 Å from the sulphur position in the EA–GSH complex. This oxygen atom is within hydrogen-bonding distance of the hydroxyl group of Tyr9 (2.8 Å). The other oxygen is able to make two hydrogen bonds, one directly to the protein to the carbonyl oxygen of Val55 (2.6 Å), and the other indirectly to the amino nitrogen of Val55 via a water molecule (B-value 38 $Å^2$). This bridging water molecule lies 2.8 Å and 3.0 Å away from the carboxylate and the amino nitrogen, respectively (Fig. 6). Although, at the pH of crystallization we would expect the carboxylate group of EA to be charged, the interaction with the carbonyl of Val55 suggests that the group has an elevated pK_a and is protonated.

A comparison of the EA and EA–GSH complexes shows that the EA is rotated by ~180° around the bond joining C3 to C4 in the phenyl ring (Fig. 7). This moves the whole molecule towards the G-site, along the plane of the dichlorophenoxy group, and causes the reactive α,β-ketone group to point away from this site. The position of the unconjugated EA, regardless of its orientation, means that the substrate is bound in a non-productive complex. It has to move in order for the glutathione to bind. Differences in the conformation of the various species along the reaction coordinate of the catalysis mediated by GST have been seen before [15]. The conformation of the tricyclohexadienate group in the transition-state analogue, 1-(*S*-glutathionyl)-2,4,6-trinitrocyclohexadienate bound to a mu-class enzyme, is significantly different to the conformation of the corresponding dinitrobenzene in the product complex, 1-(*S*-glutathionyl)-2,4-dinitrobenzene, when bound to the same enzyme. On the basis of this comparison, Ji *et al.* [15] proposed reaction coordinate motion during catalysis. The non-productive binding mode of EA that we observe, however, is probably of little consequence *in vivo* as the intracellular concentrations of glutathione (1–10 mM) are much higher than its dissociation constant (10–200 μM) and so the majority of the GST should exist in a binary complex with glutathione.

Recently, the structure of the GST from the parasitic worm *Schistosoma japonica* bound to another clinically useful drug, the anti-schistosomal drug praziquantel, has been reported [20]. The nature of inhibition of GST by praziquantel contrasts markedly with that by EA. Praziquantel does not bind to the active site but rather to the 'non-substrate-binding site' in the dimer interface where larger, non-substrate molecules such as haem are thought to bind. The drug is thought to interfere with the transport functions of the GST in addition to sterically hindering the binding of larger substrates to the H-site. These two different drug complexes represent contrasting ways of inhibiting GST.

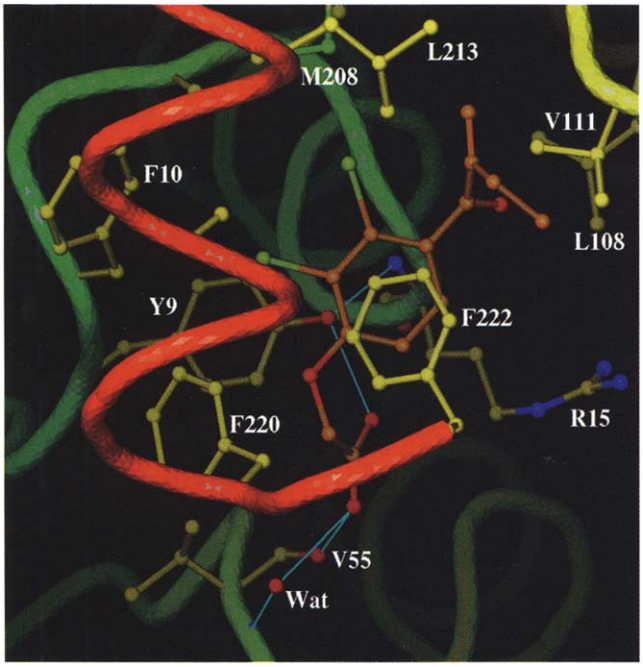

Fig. 6. View of the H-site of the EA complex. The ribbon representation of the protein has been colour ramped according to residue number as in Figure 2. The carbon atoms of the inhibitor are coloured brown to distinguish them from those of the protein, which are coloured yellow. Possible hydrogen-bonding interactions involving the inhibitor are represented by cyan lines.

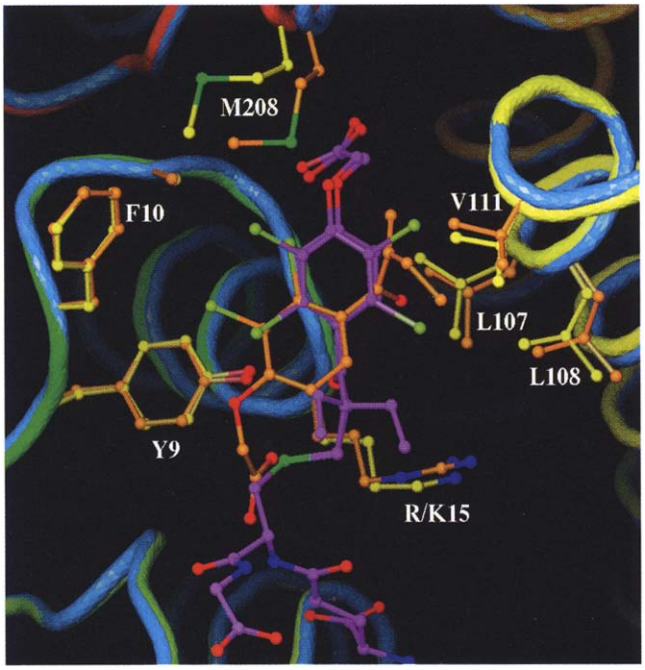

Fig. 7. Superposition of the EA complex structure on that of the EA–GSH complex showing the difference in the position of the EA moiety. Both orientations of the EA moiety in the EA–GSH complex are shown, with carbon atoms coloured magenta. The carbon atoms belonging to EA in the EA complex have been coloured brown. Protein carbon atoms are coloured yellow for the EA–GSH complex and brown for the EA complex. The ribbon representation of the Cα traces are coloured as in Figure 2 for the EA–GSH complex and blue for the EA complex. The two molecules have been superimposed using a least-squares fit of the Cα atoms of the respective monomers.

Apo-enzyme

In this study we hoped to address the important questions of, firstly, what conformational changes occur when glutathione binds to alpha-class GSTs and, secondly, how the enzyme is able to accommodate the different types of ligand. It has been postulated that when glutathione binds to the enzyme it does so by an induced-fit mechanism [7]. We observe no significant changes between the apo-enzyme and the product complexes for residues 2–207. Between residues 5 and 207 of the monomer, the rms deviation for main-chain atoms is ~0.3 Å and for all atoms is ~0.7 Å (Table 2). As the interaction between the enzyme and the glutathione appears to be highly specific, as judged from a comparison of the product complexes, we can infer from the above result that glutathione itself causes no significant conformational change at the G-site on binding. What is striking about the apo-structure, however, is the almost total absence of any electron density associated with the C-terminal α-helix. This helix, one edge of which is made up of hydrophobic residues, forms a lid over the H-site, providing a highly hydrophobic environment for the substrate [18], and has been shown to be important, though not essential, in catalysis [30]. In the structures of the complexes with benzyl–GSH, EA and EA–GSH, the helix can be observed in the electron density, although in the last two structures a number of residues are not well defined. It would appear, therefore, that the presence of a hydrophobic substrate, or possibly just glutathione, stabilizes the helix. The closure of a lid over the active site, in response to substrate binding, has been seen in a number of cases such as lactate dehydrogenase [31] and triosephosphate isomerase [32]. In these cases both open and closed conformations of the respective loops have been observed. We see no 'open' conformation and no evidence to suggest that one should occur, but rather the helix is disordered, with traces of electron density at low contour levels occurring in the usual position of the helix. None of the complexes show any specific interactions between the residues on the helix and the respective inhibitors. In the benzyl–GSH complex, the structure in which the helix is most clearly defined, only two helix residues, Phe220 and Phe222, are within van der Waals distance of the inhibitor. Phe220 is one of the best ordered side chains from the helix in the three structures where it is evident. The side chain is positioned to pack on top of the Cβ atom of the cysteinyl side chain of glutathione in a pocket made up of other aromatic residues, Tyr9 and Phe10 (Fig. 4). In the apo-structure, the conformation of Phe10 is such that it would sterically hinder Phe220 from adopting the position seen in the other three structures. There is no apparent reason, however, why Phe10, which is not well defined in any of the complex structures, should preferentially adopt this orientation. It is probably a result of the disorder of the helix rather than a cause. Regardless, it seems that the environment around Phe220 (which includes Tyr9, a residue of some importance to the

catalytic mechanism) is critical in determining whether the helix is ordered or not.

Comparison of the structures

It is mainly residues at the C terminus that are affected by the binding of the different ligands. In order to accommodate the bulkier EA–GSH conjugate, Met208, which is situated just before the C-terminal helix, has to move out of the H-site. The movement of this residue, from the position seen in all of the other structures, causes some displacement of residues further down the helix which also contribute to the formation of the H-site (Fig. 8). The conformation of the helix in the EA complex is more similar to that observed in the benzyl–GSH complex than to that in the EA–GSH complex. In neither the EA–GSH nor the EA complexes is the helix as well defined as in the benzyl–GSH complex. The average real-space correlation coefficients for the main-chain atoms of residues 208–222 are 0.85, 0.71 and 0.68 (0.85, 0.86 and 0.87 for residues 2–222), for the benzyl–GSH, EA and EA–GSH complexes, respectively. These numbers suggest that with benzyl–GSH present in the H-site, the helix is able to adopt its most 'stable' position. When EA binds to the enzyme, instead of perturbing this stable conformation unduly, it binds in a non-productive mode, partially occupying the free G-site.

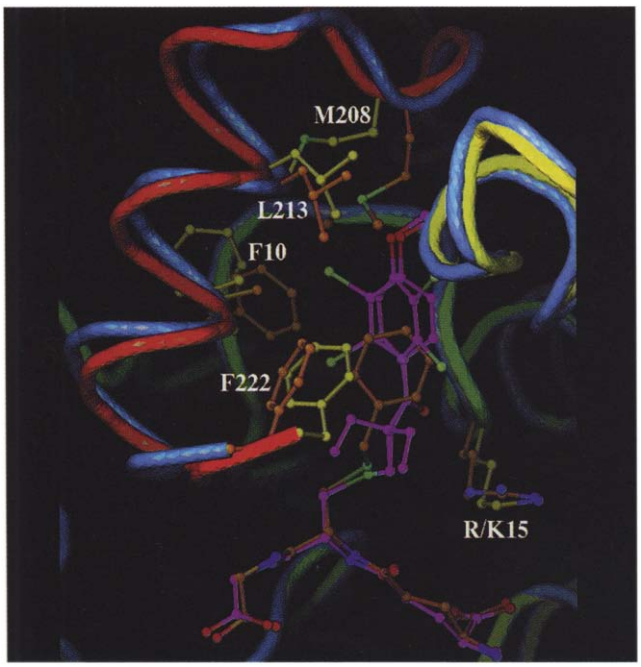

Fig. 8. Overlay of the EA–GSH and benzyl–GSH complexes showing the displacement of the C-terminal α-helix of one relative to the other. The two molecules have been superimposed based on a least-squares fit of the Cα atoms of the respective monomers. The ribbon representation of the EA–GSH complex has been colour ramped according to residue number as in Figure 2 and that of the benzyl–GSH complex is coloured light blue. Both orientations of the EA moiety of EA–GSH are shown with carbon atoms coloured magenta. The protein carbon atoms in the EA–GSH complex are coloured yellow and all carbon atoms in the benzyl–GSH complex brown.

Implications to activity

It is now reasonably well established that Tyr9, conserved throughout the alpha-, mu- and pi-class GSTs, is important in stabilizing the thiolate form of the glutathione (reviewed in [4]). There has, however, been some debate as to whether this residue could also act as a base and abstract the proton from the glutathione. García-Sáez *et al.* [13] have suggested that, should this tyrosine hydroxyl group exist in the form Tyr-O^-, some rearrangement of the active site could occur in the absence of glutathione such that a positively charged residue is brought into the environment of the negatively charged ion. We see no such arrangement in the apo-structure. Tyr9 retains the same conformation in all the structures that we have studied (e.g. Fig. 7). The only atom within hydrogen-bonding distance of the tyrosine hydroxyl group in the apo-structure is a water molecule with a relatively high B-value (45 $Å^2$). In the two EA-containing structures, the hydroxyl group is involved in hydrogen-bonding interactions with the substrate, where it must act as the hydrogen-bond donor. This suggests that Tyr9 is protonated. These results are consistent with previous crystallographic evidence where a close contact between the negatively charged sulphonate group of glutathione sulphonate and the equivalent tyrosine in the pi-class enzyme was revealed, suggesting that the hydroxyl group could not be charged [11].

The specific activity of GST A1-1 with EA is very low [2,24]. Such conjugation reactions involving α,β-unsaturated carbonyl compounds normally involve nucleophilic attack on the β-alkene carbon, C11. The reactivity of the nucleophile may be increased by a nearby base and the electrophilicity of the β-alkene carbon could also be increased by protonation of the carbonyl oxygen [2]. In GST A1-1, the only two polar residues that could possibly be involved in this mechanism are Tyr9 and Arg15. In the EA–GSH complex, the carbonyl oxygen O1 of the EA is within hydrogen-bonding distance of both of these residues (i.e. the hydroxyl of Tyr9 and the expected position for the Nϵ atom of Arg15 in the wild-type structure). As described above, the available evidence suggests that these two residues are responsible for maintaining the glutathione in the thiolate form [18,29] but they may also have an effect on the electrophilicity of the carbonyl oxygen. The mechanism could be explored more thoroughly using transition-state analogues, as in the mu-class enzyme [15]. In both the mu- and pi-class enzymes, which are more active for this class of substrate, another conserved tyrosine may be involved in this mechanism [16,33]. In the alpha-class enzymes this tyrosine is equivalent to Val111 (Figs 6,7).

Biological implications

Glutathione transferases (GSTs) help to protect the cell from potentially toxic alkylating agents that carry electrophilic functional groups, by catalyzing their conjugation with the tripeptide glutathione. The existence of multiple isoforms of GST,

together with the relatively non-specific binding of the substrate, mean that a wide variety of compounds, including certain anti-cancer drugs, can be conjugated to glutathione. Despite the considerable wealth of information in the literature about GSTs a number of questions remain unanswered concerning both the catalytic mechanism and substrate recognition. We have solved the structures of the alpha-class enzyme A1-1 in the apo-form and in complexes with both ethacrynic acid (EA) and the conjugate formed between EA and glutathione (EA–GSH). EA has been administered to cancer patients in attempts to increase the efficacy of alkylating cytostatic drugs. The rationale is that EA or EA–GSH would serve as GST inhibitors and overcome the resistance caused by GST-dependent inactivation of the cytostatic drug.

The apo-structure reported here is the first mammalian GST structure to be solved in the absence of a glutathione derivative. Comparison of the various structures reveals that no significant conformational changes occur in the glutathione binding site (G-site) of the enzyme upon binding of a glutathione derivative. On the other hand, the absence of either substrate or inhibitor from the binding site for the hydrophobic substrate (H-site) causes the C-terminal α-helix, which is unique to the alpha-class enzymes, to become disordered. The helix forms a lid over the H-site upon binding of substrate or product.

In the structure of the complex with EA, the substrate is revealed as binding in a non-productive mode, suggesting that the substrate will only form an active complex when glutathione is already bound. This is biologically sensible as the intracellular levels of glutathione are much higher than the dissociation constant of its complex with GST A1-1. Glutathione is, therefore, probably involved in the molecular recognition of the electrophilic substrate and should be considered when designing drugs to inhibit GST.

Materials and methods

Site-directed mutagenesis of GST A1-1 to generate the Arg15→Lys mutant was carried out essentially as in [34]. Recombinant protein was expressed and purified as described previously [35], with the exception that the protein was eluted from the affinity column with 50 mM glycine-NaOH, pH 10.0 rather than with *S*-hexyl-glutathione. Crystals of the apo-protein were grown using procedures similar to those of Cowan *et al.* [36]. Crystals of the enzyme in complexes with EA and EA–GSH were grown by vapour diffusion using PEG 2000 monomethyl ether as the precipitant. 3 μl of a 55 mg ml^{-1} protein solution was mixed with an equal volume of reservoir liquor containing 10–20% PEG solution, 100 mM Tris-HCl (pH 8.5), 30 mM NaAc (pH 4.6) and 1% β-mercaptoethanol. The ligand was added to the protein solution to give a final concentration of 2.5 mM. EA–GSH was obtained from a reaction between EA and reduced glutathione with no attempt to select for either of the two possible enantiomers. Crystals grew in one to two days at 20°C. Data were recorded at room temperature from the apo-crystals on a MAR imaging plate on the EMBL beamline X31 at DESY, Hamburg and processed using DENZO [37]. Data from the EA and EA–GSH complexes were collected on a Rigaku R-AXIS imaging plate mounted on a rotating anode source. The former were collected at room temperature and processed using software supplied by Rigaku [38] and the latter at 4°C and processed using DENZO [37] . A summary of the data collection methods and statistics is given in Table 3.

Refinement of the EA–GSH complex

Refinement of the EA–GSH complex was started using a model derived from the benzyl–GSH complex [18], which had undergone some preliminary refinement against the apo-enzyme data. The halving of the *c* cell dimension of the crystal of this complex with respect to that of the others (Table 3) was assumed to be caused by a slight rearrangement of the molecules in the unit cell, such that the pseudo-crystallographic symmetry described by Sinning *et al.* [18] had become crystallographic and the asymmetric unit contained one rather than two dimers. The initial model, therefore, contained one dimer without the associated water molecules. The radius of convergence of rigid-body refinement in X-PLOR [39], using data between 10 Å and 4 Å, was sufficient to correctly orient the two molecules of the dimer. To obtain the optimal non-crystallographic symmetry operators the model was subjected to a simulated annealing slow-cool protocol [40], treating both molecules independently. The refinement was then restarted using non-crystallographic symmetry constraints and thereafter a $2F_o–F_c$ map was calculated and subjected to ~10 cycles of averaging using RAVE [41]. The position of the inhibitor could be clearly seen in this map. Manual rebuilding, in which one monomer was fitted into the averaged electron density, was carried out in O [42,43]. At this stage, only the glutathione moiety of the ligand was inserted. Water molecules were included at stereochemically sensible positions where peaks were observed in the associated electron-density maps. Further refinement was carried out using alternating steps of least-squares refinement in X-PLOR (applying strict non-crystallographic symmetry constraints) and rebuilding into averaged maps. Individual atomic temperature factors were refined with tight restraints applied between bonded atoms. The free R-factor (R_{free} [44]), based on 10% of the data, was used throughout to guide the refinement procedure. During the later refinement cycles the strict non-crystallographic symmetry constraints were replaced by restraints and the two molecules of the dimer were built into unaveraged $2F_o–F_c$ maps.

The final structure of the complex between GST A1-1 and EA–GSH has an R_{cryst} of 19.7% (all data, 7.5–2.0 Å) and excellent stereochemistry (Table 4). Of the non-glycine residues, 92.6% have φ and ψ values which correspond to the most favoured regions of a Ramachandran plot [45] and no non-glycine residues lie in the disallowed regions, as defined by Morris *et al.* [46]. The four residues in the benzyl–GSH structure [18] which have pep-flip values [43] larger than 2.5 Å again have high values. Compared with the benzyl–GSH structure three peptides have been flipped: Val66, Val149 and Pro200. The final model includes all protein residues of the dimer (except for the N-terminal two residues of the B molecule, for which no density could be observed), two molecules of EA–GSH, four molecules of β-mercaptoethanol and 344 water molecules. The EA moiety of the inhibitor was

Table 3. Data processing statistics.

	EA–GSH complex	Apo-enzyme	EA complex
Space group	C2	C2	C2
Wavelength (Å)	1.54	0.92	1.54
No. of crystals	1	1	2
Data processing programs	DENZO [37]	DENZO	RAXIS [38]
Scaling program	CCP4	SCALEPACK	RAXIS/ CCP4*
Cell dimensions (a,b,c) (Å)	100.4, 94.8, 51.8, β=92.96°	100.2, 94.8 104.0, β=92.46°	101.1, 95.6 105.3, β=92.16
d_{min} (Å)	2.0	2.5	2.7
No. of observations	64 609	72 511	41 606
No. of unique reflections	30 538	31 802	26 072
Completeness (%)	93.4	97.5	94.7
R_{merge}† (%)	7.3	10.7	7.8
Reflections I>3σ (%)	88	81	80
Reflections I>3σ (%) in highest resolution shell (%)	67	61	51
Bin resolution (Å)	2.07–2.00	2.54–2.50	2.84–2.70

*Data from individual crystals were merged using the R-axis software [38] and the two data sets subsequently scaled together using the CCP4 suite of programs [47]. †$R_{merge}=\Sigma|I_{obs}-<I>|\Sigma<I>$.

Table 4. Refinement statistics of final models.

	EA–GSH complex	Apo-enzyme	EA complex
Resolution of data (Å)	7.5–2.0	7.5–2.5	7.5–2.7
R_{cryst}* (%)	19.7	23.8	22.9
R_{free} (%)	24.4	26.4	26.1
No. of atoms	4088†	1793‡	1901‡
No. of water molecules	344	104	75
Deviations from ideality§			
Bond lengths (Å)	0.009	0.010	0.010
Bond angles (°)	1.44	1.43	1.46
Dihedrals (°)	21.5	21.4	21.5
Impropers (°)	1.41	1.30	1.31
Rms B-values between bonded atoms (Å²)	2.3	3.0	–

*$R_{Cryst}=\Sigma_{hkl}||F^{obs}_{hkl}|-|F^{calc}_{hkl}||/\Sigma_{hkl}|F^{obs}_{hkl}|$. †Dimer refined with non-crystallographic symmetry restraints. ‡Monomer refined with NCS constraints to form two dimers. §Ideal parameters are those defined by Engh and Huber [48].

modelled in two conformations with relative occupancies of 0.6 and 0.4. Figure 3 shows the coordinates of the final model superimposed on an averaged $2F_o-F_c$ electron-density map calculated before the inclusion of the EA moiety in the model. The average atomic B-value of the model is 27.1 Å² (28.5 Å² for EA–GSH). There are two regions where the B-values are particularly high and the density of the maps correspondingly poor: the C-terminal α-helix of both monomers and, in the A molecule, the region comprising the loop between helices α4 and α5′ and the N-terminal portion of helix α5′. The latter is better defined in the B molecule, where it is involved in crystallographic interactions. The variation of the B-values with residue number is very similar to that of the benzyl–GSH complex [18].

A number of residues in the final model have been modelled in two conformations. One of these, Arg89, lies at the dimer interface close to a non-crytallographic symmetry related copy of itself. In the low-resolution, averaged structure of the enzyme complexed with benzyl–GSH the side chain was modelled in just one conformation such that the generation of the dimer by applying the non-crystallographic symmetry operations resulted in a close contact between the two side chains [18]. In the higher-resolution structure, it appears that the guanidino group of both residues partially occupies the same site. The two conformations modelled do not completely satisfy the electron density. Another residue modelled in two conformations is Glu104, which in the wild-type enzyme forms a salt bridge with Arg15. In the Arg15→Lys mutant the replacement of the arginine with a lysine disrupts the salt bridge and causes Glu104 to be less well defined.

In each monomer there is a strange, crescent-shaped electron density situated in a pocket lined by residues of both hydrophobic and hydrophilic nature. This pocket resides near the bottom of the crevice which is formed at the dimer interface. Although the density cannot be fully accounted for by any of the molecules within the crystallization mixture, its crescent shape is suggestive of a disulphide and, as a consequence, a 2-hydroxyethyl disulphide has been inserted. In each protein monomer one molecule of the disulphide has been modelled in two conformations. The positions of the sulphur atoms lie directly above the plane of the imidazole ring of His159.

Refinement of the apo-structure and EA complex

The starting model for the refinement of both the apo-structure and the EA complex was derived from that of the EA–GSH complex before the relaxing of the non-crystallographic symmetry constraints. The model included the full dimer with the exception of the C-terminal residues beyond Met208. EA–GSH and the β-mercaptoethanol-derived disulphide were omitted but the water molecules were included. For the apo-form, the full tetramer of the asymmetric unit was generated by placing the dimers at each of the two positions defined in a model of this structure that had undergone some preliminary refinement. For the EA complex, the tetramer was generated by duplicating the dimer at a position displaced half a unit-cell length in the direction of the *c* axis. The positions of all molecules were optimized using rigid-body refinement.

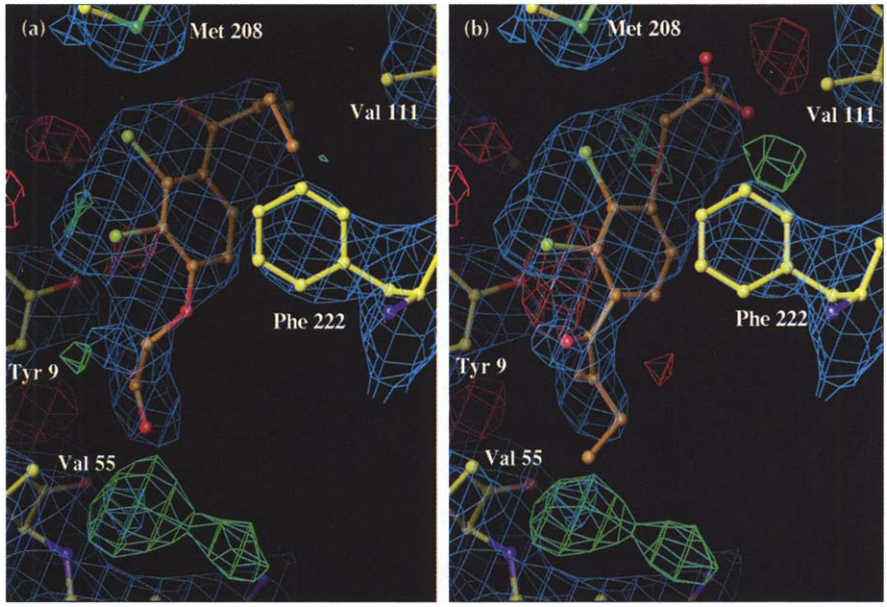

Fig. 9. Electron-density maps associated with EA after the inhibitor has been refined in each of two conformations, as described in the text. **(a)** The carboxylate pointing towards the G-site. **(b)** The α,β-ketone moiety pointing towards the G-site. The corresponding coordinates of the models have been superimposed. The $2F_o–F_c$ maps (blue) were subjected to 10 cycles of averaging (contoured at 1σ). The $F_o–F_c$ maps were averaged over the four molecules of the asymmetric unit. Positive peaks are coloured green and negative peaks are red.

Refinement of both structures was carried out in a manner similar to that described above. Strict non-crystallographic symmetry constraints were maintained throughout the refinement. The averaged $2F_o–F_c$ maps associated with the EA complex, after the initial simulated annealing slow-cool procedure, clearly revealed the position of the EA. As a result of the size similarity of the substitutions in the phenol ring, however, the quality of the density was not sufficient to define the orientation of the molecule unambiguously (i.e. either the α,β-ketone or the acetic acid moieties could point towards the G-site). Each of the possible orientations was tested by inserting EA into the model, subjecting the structure to least-squares refinement in X-PLOR, and then examining the resulting maps. In Figure 9 the coordinates of the models resulting from these tests are superimposed on the relevant maps. In each of the $F_o–F_c$ maps there is a positive peak near the ligand and within hydrogen-bonding distance of Val55. With the ligand in one conformation the peak is within hydrogen-bonding distance of the carboxylic acid group (Fig. 9a), and in the other it is very close to the non-polar α,β-ketone group (Fig. 9b). At the opposite end of the EA molecule, neither the α,β-ketone group of the former model, nor the carboxylate of the latter, completely satisfies the observed density. The surrounding residues are, however, all hydrophobic and it is more likely that the α,β-ketone group occupies this position than the polar carboxylate. Overall, therefore, we prefer the model in which the carboxylate points towards the G-site, but the limited diffraction data do not rule out the other model, or a superposition of both. For the apo-structure, individual atomic temperature factors were refined with tight restraints applied between bonded atoms, but, for the slightly lower-resolution EA structure only two temperature factors per residue were refined, corresponding to the main-chain and side-chain atoms, respectively. Refinement was terminated when no appreciable reduction in the R_{free} could be obtained with further rebuilding.

The final models of the EA complex and apo-structure have R_{cryst} values of 22.9% (7.5–2.7 Å) and 23.7% (7.5–2.5 Å), respectively. The four molecules of the asymmetric unit of each structure are identical because of the application of non-crystallographic symmetry constraints during refinement. Details of the stereochemical parameters etc. of these structures are shown in Table 4. Whereas all protein atoms have been included in the model of the EA complex, the C-terminal helix has been omitted from the apo-structure due to the absence of any associated electron density. The variation in main-chain temperature factors and the real-space fit of each residue to its associated electron density show a similar pattern to that shown by the EA–GSH complex. The average B-value for the apo-structure is 26 $Å^2$ and that for the EA complex is 43 $Å^2$ (74 $Å^2$ for EA alone). The inclusion of the C-terminal residues in the EA complex structure contributes to the higher B-value compared with that for the apo-structure. The site into which the disulphide was modelled in the EA–GSH complex again contains a crescent-shaped feature in the relevant electron-density maps. Because of the relatively low resolution of the data, however, waters were inserted rather than the molecule containing a disulphide bridge. In each structure, Arg89 appeared to make similar interactions to those described for the EA–GSH complex and was therefore modelled in two conformations.

Coordinates and structure factor amplitudes for the apo-enzyme, the EA complex and the EA–GSH complex have been deposited in the Brookhaven Protein Data Bank with entry codes 1GSD, 1GSE and 1GSF.

Acknowledgements: This work was supported by the Swedish Natural Science Research Council, the Swedish Research Council for Engineering Sciences and the Carl Trygger Foundation. GL'H. was supported by the Centre National de la Recherche Scientifique in the frame of the ATIPE grants program and by Informatique CDC. ADC was supported by the Göran Gustafsson Stiftelse.

References

1. Armstrong, R.N. (1991). Glutathione *S*-transferases: reaction mechanism, structure and function. *Chem. Res. Toxicol.* **4**, 131–140.
2. Mannervik, B. & Danielson, U.H. (1988). Glutathione transferases — structure and catalytic activity. *CRC Crit. Rev. Biochem.* **23**, 283–337.
3. Pickett, C.B. & Lu, A.Y.H. (1989). Glutathione *S*-transferase: gene structure, regulation and biological function. *Annu. Rev. Biochem.* **58**, 763–764.
4. Dirr, H., Reinemer, P. & Huber, R. (1994). X-ray crystal structures of cytosolic glutathione *S*-transferases. Implications for protein architecture, substrate recognition and catalytic function. *Eur. J. Biochem.* **220**, 645–661.
5. Wilce, M.C.J. & Parker, M.W. (1994). Structure and function of glutathione *S*-transferases. *Biochim. Biophys. Acta* **1205**, 1–18.

6. Tsuchida, S. & Sato, K. (1992). Glutathione transferases and cancer. *CRC Crit. Rev. Biochem. Mol. Biol.* **27**, 337–384.
7. Mannervik, B. (1985). The isoenzymes of glutathione transferase. *Adv. Enzymol. Rel. Areas Mol. Biol.* **57**, 357–417.
8. Mannervik, B., *et al.*, & Jörnvall, H. (1985). Identification of three classes of cytosolic glutathione S-transferase common to several mammalian species: correlation between structural data and enzymatic properties. *Proc. Natl. Acad. Sci. USA* **82**, 7202–7206.
9. Meyer, D.J., *et al.*, & Ketterer, B. (1991). Theta, a new class of glutathione transferase purified from rat and man. *Biochem. J.* **274**, 409–414.
10. Mannervik, B. & Jensson, H. (1982). Binary combinations of four protein subunits with different catalytic specificities explain the relationship between six basic glutathione *S*-transferases in rat liver cytosol. *J. Biol. Chem.* **257**, 9909–9912.
11. Reinemer, P., *et al.*, & Huber, R. (1991). The three-dimensional structure of class-pi glutathione *S*-transferase in complex with glutathione sulfonate at 2.3 Å resolution. *EMBO J.* **10**, 1997–2005.
12. Reinemer, P., *et al.*, & Parker, M.W. (1992). Three-dimensional structure of class-pi glutathione *S*-transferase from human placenta in complex with *S*-hexylglutathione at 2.8 Å resolution. *J. Mol. Biol.* **227**, 214–226.
13. García-Sáez, I., Párraga, A., Phillips, M.F., Mantle, T.J. & Coll, M. (1994). Molecular structure at 1.8 Å of mouse liver class pi glutathione *S*-transferase complex with *S*-(*p*-nitrobenzyl)glutathione and other inhibitors. *J. Mol. Biol.*, **237**, 298–314.
14. Ji, X., Zhang, P., Armstrong, R.N. & Gilliland, G.L. (1992). The three-dimensional structure of a glutathione *S*-transferase from the mu gene class. Structural analysis of the binary complex of isoenzyme 3-3 and glutathione at 2.2 Å. *Biochemistry* **31**, 10169–10184.
15. Ji, X., Armstrong, R.N. & Gilliland, G.L. (1993). Snapshots along the reaction coordinate of an S_NAr reaction catalyzed by glutathione transferase. *Biochemistry* **32**, 12949–12954.
16. Ji, X., *et al.*, & Gilliland, G.L. (1994). Structure and function of the xenobiotic substrate binding site of a glutathione *S*-transferase as revealed by X-ray crystallographic analysis of product complexes with diastereomers of 9-(*S*-glutathionyl)-10-hydroxy-9,10-dihydrophenanthrene. *Biochemistry* **33**, 1043–1052.
17. Raghunathan, S., *et al.*, & Rule, G.S. (1994). Crystal structure of human class mu glutathione transferase GSTM2-2. Effects of lattice packing on conformational heterogeneity. *J. Mol. Biol.* **238**, 815–832.
18. Sinning, I., *et al.*, & Jones, T.A. (1993). Structure determination and refinement of human alpha class glutathione transferase A1-1, and a comparison with the mu and pi class enzymes. *J. Mol. Biol.* **232**, 192–212.
19. Wilce, M.C.J., Board, P.G., Feil, S.C. & Parker, M.W. (1995). Crystal structure of a theta-class glutathione transferase. *EMBO J.* **14**, 2133–2143.
20. McTigue, M.A., Williams, D.R. & Tainer, J.A. (1995). Crystal structures of a schistosomal drug and vaccine target: glutathione *S*-transferase from *Schistosoma japonica* and its complex with the leading antischistosomal drug praziquantel. *J. Mol. Biol.* **246**, 21–27.
21. van Ommen, B., Bogaards, J.J.P., Peters, W.H.M., Blaauboer, B. & van Bladern, P.J. (1990). Quantification of human hepatic glutathione S-transferases. *Biochem J.* **269**, 609–613.
22. Smith, M., *et al.*, & Mannervik, B. (1989). Denitrosation of 1,3-bis(2-chloroethyl)-1-nitrosourea by class mu glutathione transferases and its role in cellular resistance in rat brain tumour cells. *Cancer Res.* **49**, 2621–2625.
23. Hansson, J., *et al.*, & Ringborg, U. (1991). Sensitization of human melanoma cells to the cytotoxic effect of melphalan by the glutathione transferase inhibitor ethacrynic acid. *Cancer Res.* **51**, 94–98.
24. Ploemen, J.H.T.M., van Ommen, B., Bogaards, J.J.P. & van Bladeren, P. J. (1993). Ethacrynic acid and its glutathione conjugate as inhibitors of glutathione S-transferases. *Xenobiotica* **23**, 913–923.
25. Tew, K.D., Bomber, A.M. & Hoffman, S.J. (1988). Ethacrynic acid and piriprost as enhancers of cytotoxicity in drug resistance and sensitive cell lines. *Cancer Res.* **48**, 3633–3625.
26. Clapper, M.L., Hoffman, S.J. & Tew, K.D. (1990). Sensitisation of human colon tumor xenografts to phenylalanine mustard using ethacrynic acid. *J. Cell. Pharmacol.* **1**, 71–78.
27. O'Dwyer, P.J., *et al.*, & Ozols, R.E. (1991). Phase I study of thiotepa in combination with the glutathione transferase inhibitor ethacrynic acid. *Cancer Res.* **51**, 6059–6065.
28. Ranganathan, S., Ciaccio, P.J. & Tew, K.D. (1993). Principles of drug modulation applied to glutathione S-transferases. In *Structure and Function of Glutathione Transferases.* (Tew, K.D., Pickett, C.B., Mantle, T.J., Mannervik, B., & Hayes, J.D., eds), pp. 249–256, CRC Press Inc., Boca Raton, FL.
29. Mannervik, B., *et al.*, & Widersten, M. (1993). Structural and functional characterization of the binding sites for glutathione (G-site) and the hydrophobic electrophilic substrate (H-site) in glutathione transferases. In *Structure and Function of Glutathione Transferases.* (Tew, K.D., Pickett, C.B., Mantle, T.J., Mannervik, B., & Hayes, J.D., eds.), pp. 29–38, CRC Press Inc., Boca Raton, FL.
30. Board, P. G. & Mannervik, B. (1991). The contribution of the C-terminal sequence to the catalytic activity of GST2, a human alpha-class glutathione transferase. *Biochem. J.* **275**, 171–174.
31. Grau, U., Tommer, W. & Rossmann, M. (1981). Structure of the active ternary complex of pig heart lactate dehydrogenase with *S*-lac-NAD at 2.7 Å resolution. *J. Mol. Biol.* **151**, 289–307.
32. Lolis, E. & Petsko, G. (1990). Crystallographic analysis of the complex between triosephosphate isomerase and 2-phosphoglycolate at 2.5 Å resolution. *Biochemistry* **29**, 6609–6625.
33. Johnson, W.W., Liu, S., Ji, X., Gilliland, G.L. & Armstrong, R.N. (1993). Tyrosine 115 participates both in chemical and physical steps of the catalytic mechanism of a glutathione S-transferase. *J. Biol. Chem.* **268**, 11508–11511.
34. Stenberg, G., Board, P.G., Carlberg, I. & Mannervik, B. (1991). Effects of directed mutagenesis on conserved residues in a human class alpha glutathione transferase. *Biochem. J.* **274**, 549–555.
35. Stenberg, G., Björnestedt, R. & Mannervik, B. (1992). Heterologous expression of recombinant human glutathione transferase A1-1 from a hepatoma cell line. *Protein Express. Purif.* **3**, 80–84.
36. Cowan, S.W., *et al.*, & Mannervik, B. (1989). Crystallization of GST2, a human class alpha glutathione transferase. *J. Mol. Biol.* **208**, 369–370.
37. Otwinowski, Z. (1993). Oscillation data reduction program. In *Data Collection and Processing.* (Sawyer, L., Isaacs, N. & Bailey, S., eds), pp. 56–63, SERC Daresbury Laboratory, Warrington, UK.
38. Sato, M., Yamamoto, M., Imada, K. & Katsube, Y.J. (1992). A high-speed data collection system for large unit cell crystals using an imaging plate as a detector. *J. Appl. Crystallogr.* **25**, 348–357.
39. Brünger, A.T. (1990). *X-PLOR: A system for Crystallography and NMR.* Yale University Press, New Haven, CT.
40. Brünger, A.T. & Krukowski, A. (1990). Slow-cooling protocols for crystallographic refinement by simulated annealing. *Acta Crystallogr. A* **46**, 585–593.
41. Kleywegt, G. & Jones, T. (1994). Halloween... masks and bones. In *From First Map to Final Model.* (Bailey, S., Hubbard, R. & Waller, D., eds), pp. 59–66, EPSRC, Daresbury Laboratory, Warrington, UK.
42. Jones, T.A. & Kjeldgaard, M. (1991). *O, The Manual.* pp. 1–166, Uppsala, Sweden.
43. Jones, T.A., Zou, J.Y., Cowan, S.W. & Kjeldgaard, M. (1991). Improved methods for building protein models in electron density maps and the location of errors in these models. *Acta Crystallogr. A* **47**, 110–119.
44. Brünger, A.T. (1992). Free R value: a novel statistical quantity for assessing the accuracy of crystal structures. *Nature* **355**, 472–475.
45. Ramakrishnan, C. & Ramachandran, G.N. (1965). Stereochemical criteria for polypeptide and protein chain conformation. *Biophys. J.* **5**, 909–933.
46. Morris, A.L., MacArthur, M.W., Hutchinson, E.G. & Thornton, J.M. (1992). Stereochemical quality of protein structure coordinates. *Proteins* **12**, 345–365.
47. Collaborative Computation Project Number 4 (1994). The CCP4 Suite: programs for protein crystallography. *Acta Crystallogr. D* **50**, 760–763.
48. Engh, R.A. & Huber, R. (1991). Accurate bond and angle parameters for X-ray protein structure refinement. *Acta Crystallogr. A* **47**, 392–400.

Received: **24 Apr 1995**; revisions requested: **12 May 1995**; revisions received: **2 Jun 1995**. Accepted: **2 Jun 1995**.